

Projektarbeit Hart- u. Weichmagnete

LV-Nr. 131.019

Calculation of eddy currents in metal samples

ausgeführt am Institut für Experimentalphysik
der Technischen Universität Wien

unter der Anleitung von
Ao.Univ.Prof. Dipl.-Ing. Dr.techn. Roland Grössinger
und Univ. Doz. Dr. Thomas Schrefl

durch

Werner Scholz
Margaretengürtel 62-64/63/3
1050 Wien

Wien, September 1999

korrigierte Version: Juli 2001

<http://magnet.atp.tuwien.ac.at/scholz/projects/proj3/>

CONTENTS

1 MAXWELL'S EQUATIONS	6
2 THE FINITE ELEMENT METHOD	9
3 BOUNDARY CONDITIONS	11
4 FEMM	13
4.1 2D simplifications	14
4.2 Axisymmetric problems	14
4.3 Program test	14
5 EXPERIMENTAL SETUP	16
5.1 Field coil	16
5.2 Samples	17
6 FINITE ELEMENT MODELS	18
6.1 Single turn coil	18
6.2 Detailed coil model	18
7 MAGNETIC FIELD	20
7.1 Single turn coil	20
7.2 Detailed coil model	22
8 EDDY CURRENTS	24
8.1 Sample Cu1 (cylindrical)	24
8.1.1 Single turn coil	25
8.1.2 Coil model	25
8.2 Sample Al3 (spherical)	28
8.3 Sample Cu3	29
8.4 Comparison of experimental and numerical results	30
9 INDUCED MAGNETIC MOMENT	31
9.1 Cylindrical samples	31

	3
9.2 Spherical samples	31
10 EDDY CURRENTS IN A SOLID SPHERE	33
10.1 Analytical solution	33
10.2 Numerical solution	35
10.3 Sample Cu3	38
10.4 Frequency dependence	39
11 COMMENTS ON RELEASE 2.1A OF FEMM	41
12 CONCLUSIONS	42
13 REFERENCES	43
14 LIST OF MODELS	46
14.1 Subdirectory test	46
14.1.1 turn.FEM	46
14.1.2 coilturn.FEM	46
14.2 Subdirectory experiment	46
14.2.1 singturn.FEM	46
14.2.2 singturnsphere.FEM	46
14.2.3 singturnfsphere.FEM	46
14.2.4 cylinder.FEM	46
14.2.5 sphere.FEM	46
14.2.6 miniturnsphere.FEM	47
14.2.7 sphereref.FEM	47
15 APPENDIX	48
15.1 Mathematica package sphere.nb	48
15.2 David Meeker, Finite Element Method Magnetics. User's Manual	49

List of Figures

Figure 1: User interface of the preprocessor	13
Figure 2: Induction in radial distance from the symmetry axis	15
Figure 3: Single turn coil	18
Figure 4: Detailed coil model.....	19
Figure 5: Finite element mesh of the single turn coil.....	20
Figure 6: Flux lines of a single turn coil with static current.....	21
Figure 7: Flux lines of a single turn coil with harmonic current	22
Figure 8: Finite element mesh of the detailed coil model.....	23
Figure 9: Flux lines of the detailed coil model.....	23
Figure 10: Magnetic field due to a current pulse in the field coil	24
Figure 11: Complex eddy current density as a function of radial distance from axis.....	25
Figure 12: Complex eddy current density as a function of radial distance from axis (10 Hz).....	25
Figure 13: Complex eddy current density at a constant distance of 0.1 cm from axis (10 Hz).....	26
Figure 14: Complex eddy current density as a function of radial distance from axis (112 Hz).....	26
Figure 15: Complex eddy current density at a constant distance of 0.1 cm from axis.....	26
Figure 16: High resolution mesh of the cylindrical sample	27
Figure 17: Complex eddy current density as a function of radial distance from axis.....	27
Figure 18: Complex eddy current density at constant distance from axis	28
Figure 19: High resolution mesh of the spherical sample	28
Figure 20: Complex eddy current density as a function of radial distance from axis (centre of the sphere)	28
Figure 21: Complex eddy current density as a function of radial distance from axis (at $r=1.25$ mm)	29
Figure 22: Complex eddy current density at constant distance from axis (1.25 mm)	29
Figure 23: High resolution mesh of the spherical sample	29
Figure 24: Complex eddy current density as a function of radial distance from axis (centre of the sphere)	30
Figure 25: FE mesh (small cut out) of the iron sphere and detailed coil model.....	35
Figure 26: Magnetic induction in the iron sphere	36
Figure 27: Eddy current density in the iron sphere	36
Figure 28: Eddy current density in the iron sphere	37

Figure 29: Eddy current density in the iron sphere	37
Figure 30: Eddy current density in sample Cu2 @ 1 T	38
Figure 31: Eddy current density in sample Cu2 @ 1 T	39
Figure 32: Eddy current density in sample Cu2 @ 5.17 T	39

List of Tables

Table 1: FEMM results for FE meshes with different density	15
Table 2: Field coil specifications	16
Table 3: Specifications of the samples	17
Table 4: Magnetic field of the single turn coil	20
Table 5: Magnetic field of the detailed coil model.....	22
Table 6: Comparison of experimental and numerical results	30
Table 7: Comparison of experimental and numerical results	40

1 Maxwell's equations

Until the 19th century electric and magnetic effects were seen as two independent physical occurrences. In 1820 Oersted proved, that electric currents can influence the needle of a compass. Ampère and Faraday laid the foundation for the unified theory of electrodynamics, which was elaborated by James Clerk Maxwell (1831-1879).

His famous equations are the starting point for our investigations:

$$\begin{aligned}
 \operatorname{div} \vec{D} &= \rho \\
 \operatorname{div} \vec{B} &= 0 \\
 \operatorname{curl} \vec{E} &= -\frac{\partial \vec{B}}{\partial t} \\
 \operatorname{curl} \vec{H} &= \frac{\partial \vec{D}}{\partial t} + \vec{j}
 \end{aligned} \tag{1}$$

In order to solve these equations for our purpose, we have to make several assumptions. First, we neglect any displacement currents $\vec{D} = \varepsilon_0 \varepsilon \vec{E}$, which are typically relevant only at radio frequencies (in the MHz regime), and set $\varepsilon = 1$. In the quasistatic approximation we omit the term

$$\frac{\partial \vec{D}}{\partial t} . \tag{2}$$

Secondly, we assume, that there are no free charges ρ . The simplified Maxwell equations are given by

$$\begin{aligned}
 \operatorname{div} \vec{E} &= 0 \\
 \operatorname{div} \vec{B} &= 0 \\
 \operatorname{curl} \vec{E} &= -\frac{\partial \vec{B}}{\partial t} \\
 \operatorname{curl} \vec{H} &= \vec{j}
 \end{aligned} \tag{3}$$

Then, we require the field intensity \vec{H} and the flux intensity \vec{B} to obey the constitutive relationship

$$\vec{B} = \mu \vec{H} . \tag{4}$$

If the material is nonlinear (e.g. ferromagnetic), the permeability μ is a function of B .

$$\mu = \frac{B(H)}{H} \tag{5}$$

However, we will consider only linear materials in this project.

The relationship between the electric field intensity \vec{E} and the current density \vec{j} is given by

$$\vec{j} = \sigma \vec{E}. \quad (6)$$

Now we introduce a magnetic vector potential \vec{A} , and define it as

$$\vec{B} = \text{curl} \vec{A} \quad (7)$$

which guarantees the validity of Maxwell's second equation. Then we can rewrite the fourth equation and obtain

$$\text{curl} \left(\frac{1}{\mu} \text{curl} \vec{A} \right) = \vec{j} \quad (8)$$

With the Coulomb gauge condition

$$\text{div} \vec{A} = 0 \quad (9)$$

and the well known operator relation

$$\text{curl}(\text{curl} \vec{A}) = \text{grad}(\text{div} \vec{A}) - \text{div}(\text{grad} \vec{A}) \quad (10)$$

we find

$$-\frac{1}{\mu} \text{div}(\text{grad} \vec{A}) = \vec{j}. \quad (11)$$

Inserting (7) in the third Maxwell equation yields

$$\text{curl} \vec{E} = -\text{curl} \frac{\partial \vec{A}}{\partial t}. \quad (12)$$

In the case of 2D problems, we can integrate this equation and get

$$\vec{E} = -\frac{\partial \vec{A}}{\partial t} \quad (13)$$

and together with the constitutive relationship between the electric field intensity \vec{E} and the current density \vec{j} we obtain

$$\vec{j} = -\sigma \frac{\partial \vec{A}}{\partial t} \quad (14)$$

Finally we insert this in (11) to eliminate \vec{j} and arrive at

$$\frac{1}{\mu} \text{div}(\text{grad} \vec{A}) = \sigma \frac{\partial \vec{A}}{\partial t} - \vec{j}_{src}, \quad (15)$$

where \vec{j}_{src} represents the applied current sources.

Finally, we restrict ourselves to time harmonic problems, in which all fields oscillate harmonically at one fixed frequency. Thus, we can use a phasor transformation and rewrite the magnetic vector potential as

$$\vec{A} = \text{Re}[\vec{a}(\cos \omega t + i \sin \omega t)] = \text{Re}[\vec{a}e^{i\omega t}] \quad (16)$$

in which \vec{a} is the complex amplitude. By substituting this ansatz in (15) we can eliminate the time derivative and finally arrive at

$$\frac{1}{\mu} \text{div}(\text{grad} \vec{a}) = i\omega\sigma \vec{a} - \vec{j}_{src}. \quad (17)$$

2 The finite element method

The finite element method has become a well established method in many fields of computer aided engineering, such as structural analysis, fluid dynamics, and electromagnetic field computation.

There are three main steps during the solution of a partial differential equation (PDE) with the finite element method. First, the domain, on which the PDE should be solved, is discretized into finite elements. Depending on the dimension of the problem this can be triangles, squares, rectangles, or tetrahedrons, cubes, or hexahedrons. The solution of the PDE is approximated by piecewise continuous polynomials and the PDE hereby discretized and split into a finite number of algebraic equations. Thus, the aim is to determine the unknown coefficients of these polynomials in such a way, that distance (which is defined by the norm in a suitable vector space) from the exact solution becomes a minimum. Therefore, the finite element method is essentially a variational minimization technique.

Since the number of elements is finite, we have reduced the problem of finding a continuous solution for our PDE to calculating the finite number of coefficients of the polynomials. The solution of Poisson's equation (17), which is required to calculate the magnetic vector potential, has to be solved for a given current density distribution. We write Poisson's equation in a more general form

$$\Delta u(\vec{r}) = f(\vec{r}). \quad (18)$$

In order to apply the finite element method, we have to find a variational formulation.

The Galerkin method leads to the *weak formulation* of the problem: We multiply Poisson's equation by a test function $v(r)$ and integrate over the solution domain

$$\int_{\Omega} \Delta u(\vec{r}) v(\vec{r}) d\vec{r} = \int_{\Omega} f(\vec{r}) v(\vec{r}) d\vec{r}. \quad (19)$$

Integration by parts gives

$$-\int_{\Omega} \nabla u(\vec{r}) \nabla v(\vec{r}) d\vec{r} + \int_{\Gamma} \nabla u(\vec{r}) v(\vec{r}) d\vec{r}_n = \int_{\Omega} f(\vec{r}) v(\vec{r}) d\vec{r}. \quad (20)$$

where \vec{r}_n denotes the surface normal on the boundary Γ . If appropriate boundary conditions define the values of u (Dirichlet boundary conditions) or of its derivatives $\nabla u =: g$ (Neumann boundary conditions) on the boundary, we can simplify (since v vanishes, where Dirichlet boundary conditions apply)

$$-\int_{\Omega} \nabla u(\vec{r}) \nabla v(\vec{r}) d\vec{r} + \int_{\Gamma_n} g v(\vec{r}) d\vec{r}_n = \int_{\Omega} f(\vec{r}) v(\vec{r}) d\vec{r}. \quad (21)$$

The exact solution $u(r)$ shall be approximated by a linear combination of trial functions $\varphi_i(\vec{r})$

$$u_h(\vec{r}) = \sum_{i=0}^n u_i \varphi_i(\vec{r}). \quad (22)$$

and we use a finite set of test functions v_i .

If we insert this expansion in (21) and assume only Dirichlet boundary conditions

$$\sum_{i=0}^n u_i \int \nabla \varphi_i(\vec{r}) \nabla v_i d\vec{r} = \int f(\vec{r}) d\vec{r}. \quad (23)$$

we get a system of algebraic equations.

This can be solved with any standard method for the solution of a system of algebraic equations, such as the Gauß method, the Cholesky decomposition or iterative schemes like the conjugate gradient method.

3 Boundary conditions

For the solution of partial differential equations like Maxwell's equations, we need boundary conditions to find a unique solution. There are three types of boundary conditions:

Dirichlet boundary conditions

The value of the solution is explicitly defined on the boundary (or part of it). The magnetic vector potential is usually set to zero along a boundary, which should not be crossed by magnetic flux.

Neumann boundary conditions

The normal derivative of the solution is defined on the boundary. If we set the normal derivative of the magnetic vector potential to zero, the boundary can be interpreted as an interface with a highly permeable metal. Then, the magnetic flux passes the interface at an angle of 90° to the plane of the interface. In order to find a unique solution, a Dirichlet boundary condition must be defined somewhere on the boundary of the domain.

Robin boundary conditions

A combination of the first two boundary conditions is called a Robin boundary condition. In this case the normal derivative of the solution and the value of the solution itself on the boundary are connected by a function.

Asymptotic boundary conditions

For many problems neither of the two boundary conditions above is suitable: Natural boundary conditions usually set the solution to a distinct value at infinity. However, finite element methods, can only handle finite domains to solve the problem in a computer at finite speed with finite memory.

One workaround is the truncation of outer boundaries. At an arbitrary distance "far enough away" from the area of interest Dirichlet or Neumann boundary conditions are applied. This is very simple, but not very accurate. In addition, it is quite inefficient, because a volume of air, which is much larger than the area of interest, has to be modeled. A fine mesh in the area of interest and a coarse mesh in the exterior can reduce the computational effort again.

Asymptotic boundary conditions transform natural boundary conditions into Robin boundary conditions on the surface of a finite domain. This is achieved by developing the solution into a series expansion of spherical harmonics.

$$A(r, \theta) = \sum_{m=1}^{\infty} \frac{a_m}{r^m} \cos(m\theta + \alpha_m) \quad (24)$$

Only the leading harmonic

$$A(r, \theta) \approx \frac{a_n}{r^n} \cos(n\theta + \alpha_n) \quad (25)$$

is considered, since higher order harmonics decay very quickly.

We get the normal derivative on a spherical surface by differentiating with respect to r . Solving for a_n and substituting into (25) gives

$$\frac{\partial A}{\partial r} + \left(\frac{n}{r}\right)A = 0 \quad (26)$$

If the outer edge of the solution domain is circular the open domain solution can be closely approximated by applying (26) at the boundary $r = r_b$, which should be at least 5 times the radius of the area of interest.

4 FEMM

The finite element package FEMM by David Meeker [3] provides a complete set of tools for solving static and low frequency 2D or axisymmetric problems in electrodynamics. Like any typical FE package it consist of the following three parts:

Preprocessor

The preprocessor (`femme.exe`) is a simple CAD program for defining the geometry of the problem, material properties, mesh densities and boundary conditions. The finite element mesh can be created and viewed. Figure 1 shows a snapshot of the preprocessor with a model of the single turn coil (cf. section 6.1). The horizontal axis is the r -axis and the vertical axis is the z -axis. The small dot in the middle on the left border, which is the symmetry axis, is the sample and to its right the cross section of the single turn coil is visible. The semi-circle denotes the boundary, where asymptotic boundary conditions are applied. In all following figures this ($r > 0, z$) plane with the asymptotic boundary will be displayed.

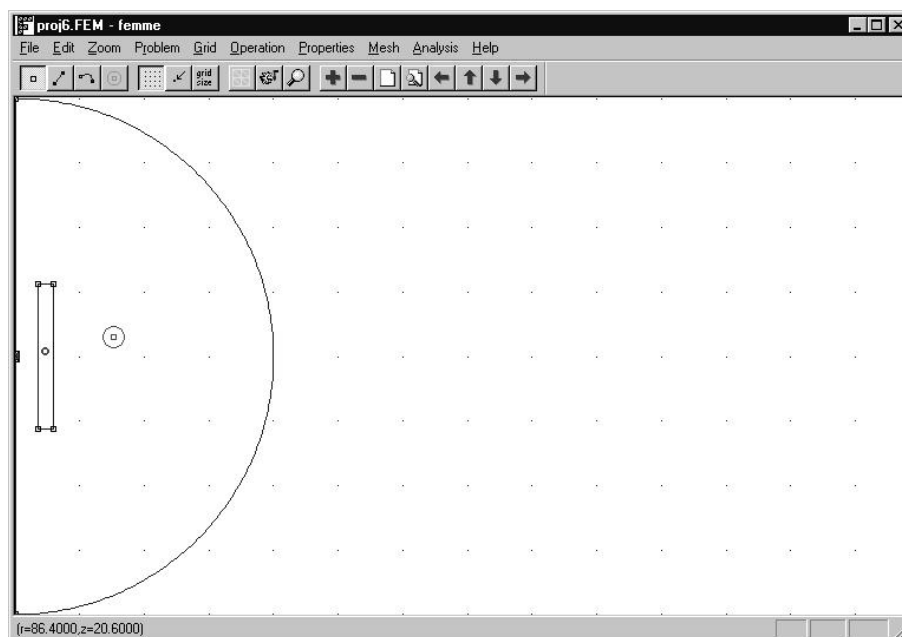


Figure 1: User interface of the preprocessor

Solver

The solver (`fkern.exe`) reads the information defined during the preprocessing step and solves Maxwell's equations.

Postprocessor

The postprocessor (`femview.exe`) displays the results as density and contour plots. In addition the user can inspect the solution at any point, plot interesting results in graphs and calculate certain integrals.

4.1 2D simplifications

In general, the magnetic vector potential is a 3D vector with three non-vanishing components. However, in 2D planar and axisymmetric cases two of these components are zero. Only the “out of plane” component is non-zero. The vector potential approach has the advantage, that only one equation (8) or (11) has to be solved. The magnetic field and the magnetic induction can be deduced by differentiating the vector potential. In addition, (8) is an elliptic partial differential equation. This is a well known and thoroughly studied type, which occurs in many engineering problems.

4.2 Axisymmetric problems

In axisymmetric problems the magnetic vector potential must vanish at $r = 0$. Thus, we do not have to define any other Dirichlet boundary conditions, if $r = 0$ is part of the domain boundary.

4.3 Program test

The finite element package FEMM has been tested by calculating the magnetic field of a single turn coil with constant current. The results can easily be compared with the analytic solution.

inner diameter:	5 cm
coil area S:	78,54 cm ²
cross section:	0.2×0.2 cm ² = 0.04 cm ² = 4e-6 m ²
current density:	1 MA/m ²
total current:	4 A

The magnetic induction B at $r = 0$ in the centre of the coil is given by [4]

$$B = \frac{\mu_o IR^2}{2(R^2 + h^2)^{3/2}} \quad (27)$$

With the data given above we get $B = 5.0265e-5$ T. (The cross section of the coil has been neglected.)

With FEMM we get the following results:

nodes	elements	B (T)
2673	5077	5.03e-5
5229	10161	4.92e-5
10264	20053	4.96e-5
27870	55103	4.93e-5

Table 1: FEMM results for FE meshes with different density

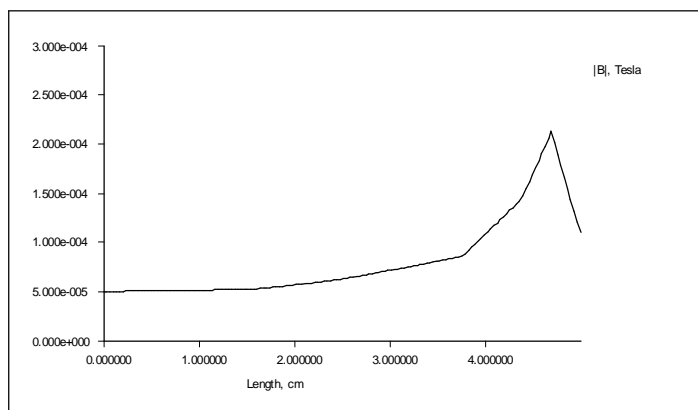


Figure 2: Induction in radial distance from the symmetry axis

5 Experimental setup

5.1 Field coil

Cu wire: $5 \times 9 \text{ mm}^2$ cross section
 specific resistivity: $1.79 \cdot 10^{-8} \Omega\text{m}$
 specific conductivity: 55.866 MS/m
 insulation: 0.15 mm glasfibre-epoxy

coil dimensions:

inner diameter: 70 mm

layers: 2 or 4

turns/layer: 24

layers		2*	4*
resistivity (measured)	[mΩ]	4.91	10.91
inductivity (measured, 120 Hz)	[μH]	53.3	242.3
homogeneity (50 mm)	[%]	0.85	1
damping 2nd halfwave	[%]	30	25
maximum field 2200 V, 8 mF	[T]	5.9 (4.1)	5.7 (4.3)
maximum field 2200 V, 24 mF	[T]	9.6 (6.7)	9.3 (6.9)
maximum current 2200 V, 8 mF	[kA]	23.4 (19)	11.4 (9.7)
maximum current 2200 V, 24 mF	[kA]	38 (26.6)	18.7 (14)
pulse duration 2200 V, 8 mF	[ms]	4.3	9.1
pulse duration 2200 V, 24 mF	[ms]	7.5	15.7

Table 2: Field coil specifications

*) the values for the second halfwave are given in brackets

5.2 Samples

	units	Cu1	Cu2	Cu3	Al1	Al2	Al3
shape		cylinder	cylinder	sphere	cylinder	cylinder	sphere
height	mm	8	8		8	8	
diameter	mm	4	4	7,3	4	4	5
volume	mm ³	101	101	203,69	101	101	65,45
weight	g		0,90926	1,81008		0,28055	0,1877
spec. resistivity	$\Omega\text{mm}^2/\text{m}$	0,01724	0,0176	0,0176	0,052	0,0382	0,0382
spec. conductivity	MS/m	58,00	56,82	56,82	19,23	26,18	26,18

Table 3: Specifications of the samples

The data given by WebElements [6] for bulk material are:

Cu

specific resistivity: $1.7\text{e-}8 \Omega\text{m}$

specific conductivity: 58.82 MS/m

density: $8920 \text{ kg/m}^3 = 8.920 \text{ g/cm}^3$

Al

specific resistivity: $2.65\text{e-}8 \Omega\text{m}$

specific conductivity: 37.74 MS/m

density: $2700 \text{ kg/m}^3 = 2.700 \text{ g/cm}^3$

6 Finite element models

Since the external field cannot be defined explicitly in FEMM, we have to model a coil to generate the magnetic field. Two different models have been tested. First, a coil of a single turn, whose dimensions are equivalent to the outer dimension of the field coil, which has been used in the experiments. Secondly, a detailed model of the coil with 4 layers of 24 windings each has been created.

6.1 Single turn coil

inner diameter: 70 mm
 outer diameter: 120 mm
 height: 226 mm
 cross section: $11300/2 = 5650 \text{ mm}^2$

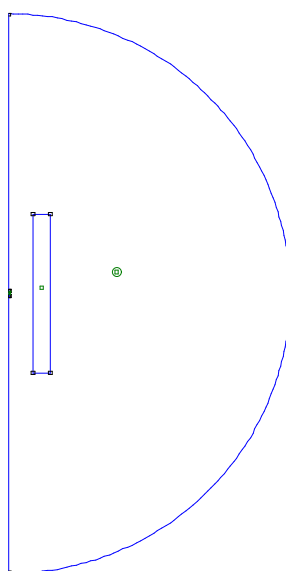


Figure 3: Single turn coil

6.2 Detailed coil model

4 layers of 24 turns each
 cross section: $4 \times 9 \text{ mm}^2$
 total cross section: $4 \times 24 \times 36 \text{ mm}^2 = 3456 \text{ mm}^2$

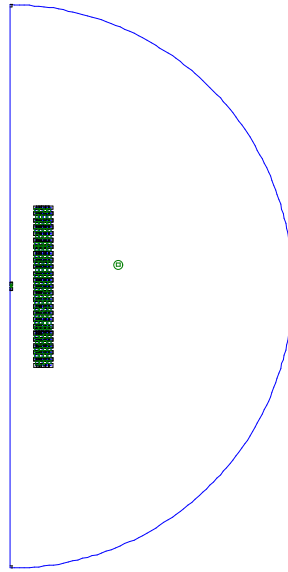


Figure 4: Detailed coil model

7 Magnetic field

A test for FEMM is the calculation of the magnetic field, which is generated by the field coil. The experimental data are given in table 1.

7.1 Single turn coil

A mesh of 705 nodes and 1186 elements has been used to calculate the field on the axis in the centre of the coil. A static current was assumed.

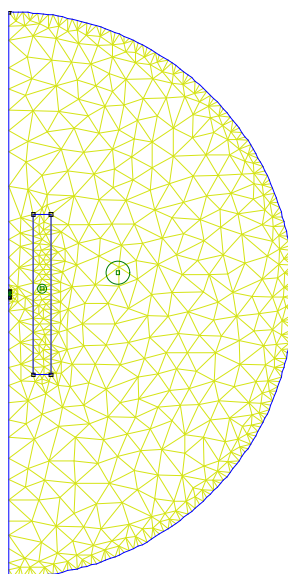


Figure 5: Finite element mesh of the single turn coil

maximum current	layers	capacity	current density	total current	maximum field	current/field ratio	calculated field	current/field ratio
kA		mF	MA/m ²	kA	T		T	
9,70	4	8	164,81	931,20	4,30	216,56	4,80	193,96
11,40	4	8	193,70	1094,40	5,70	192,00	5,64	193,94
14,00	4	24	237,88	1344,00	6,90	194,78	6,93	193,94
18,70	4	24	317,73	1795,20	9,30	193,03	9,26	193,95
19,00	2	8	161,42	912,00	4,10	222,44	4,70	193,92
23,40	2	8	198,80	1123,20	5,90	190,37	5,79	193,96
26,60	2	24	225,98	1276,80	6,70	190,57	6,58	193,95
38,00	2	24	322,83	1824,00	9,60	190,00	9,41	193,94

Table 4: Magnetic field of the single turn coil

The results of the calculations are in agreement with the experimental values. In the numerical simulation, the current to field ratio is constant (which we expect for a constant current density over the cross section of the coil) and in good agreement with the experimentally measured data. There are only two data sets (both of them are data of the second halfwave with the 8 mF capacitor), for which the current/field ratio is too high. This can be explained by the fact, that

the experimental setup includes a free RLC oscillator circuit, which generates a damped pulse. The damping has to be considered, when calculating the field. However, our harmonic approximation cannot take this into account.

If a harmonic current with a frequency of 112 Hz is applied, the induction on the axis drops to an amplitude of 0.4238 T for a maximum current of 11.4 kA. The reason is, that the harmonic analysis solves the quasistatic problem and includes self inductance and eddy currents within the coil. However, the current pulse in the experiment lasts for only one period. Thus, the system cannot reach equilibrium. In order to avoid this effect, the conductivity of the coil has been set to zero in all following calculations. As FEMM still allows us to define a current, we get rid of the above mentioned effects.

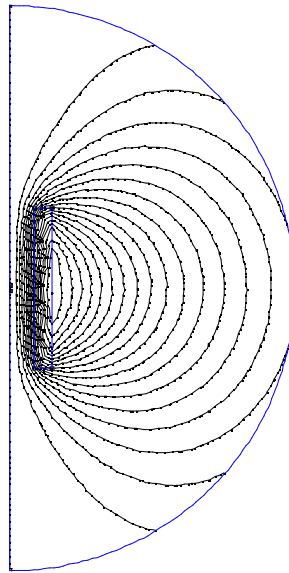


Figure 6: Flux lines of a single turn coil with static current

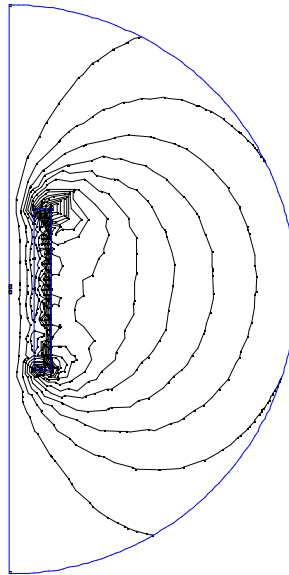


Figure 7: Flux lines of a single turn coil with harmonic current

7.2 Detailed coil model

With the detailed model of the coil, which consists of 4 layers of 24 turns each, the results given in table 5 were obtained. Once again we find differences between experiment and simulation for one data set, which has already been discussed in the previous section.

maximum current	current density	maximum field	current/field ratio	calculated field	current/field ratio
kA	MA/m ²	T		T	
9,70	4 269,44	4,30	2,26	4,80	2,02
11,40	4 316,67	5,70	2,00	5,64	2,02
14,00	4 388,89	6,90	2,03	6,93	2,02
18,70	4 519,44	9,30	2,01	9,26	2,02

Table 5: Magnetic field of the detailed coil model

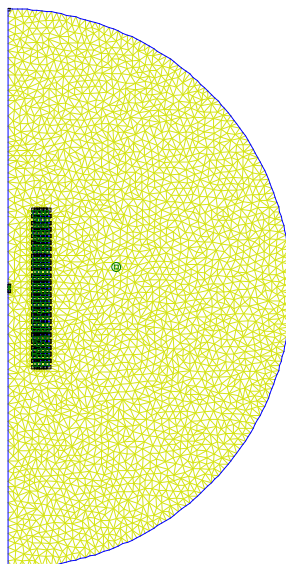


Figure 8: Finite element mesh of the detailed coil model

The finite element mesh consists of 6108 nodes and 11946 elements.

For a harmonic current of 11.4 kA at 112 Hz with a conductivity of 55.8659 MS/m of the coil, the induction on the symmetry axis in the centre of the coil drops to an amplitude of 0.4123 T.

If we set the conductivity of coil to zero we find an amplitude of 5.64 T for the induction.

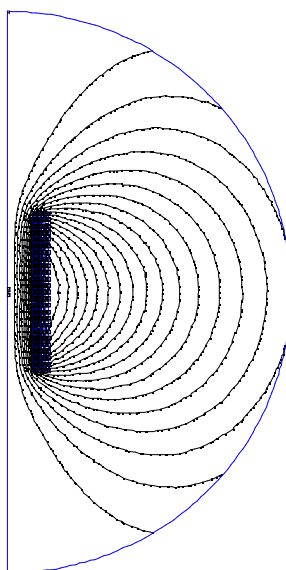


Figure 9: Flux lines of the detailed coil model

8 Eddy currents

The experimental setup consists of a big condenser battery, which powers the field coil described in section 5.1. The discharge of the condenser batteries runs through an RLC oscillator and the field coils, which generate the magnetic field. The magnetic field as a function of time is shown in figure 10 for a typical discharging process. It has (approximately) the shape of a damped sine. Thus, it seems to be sensible, if we make a time harmonic analysis and compare the results with the pulse field experiments. The magnetic field reaches a maximum value of 5.23 T and a minimum value of 4.29 T. The time from the beginning until the end of the sinusoidally varying field is approximately 0.008864 s, which corresponds to a frequency of 112 Hz.

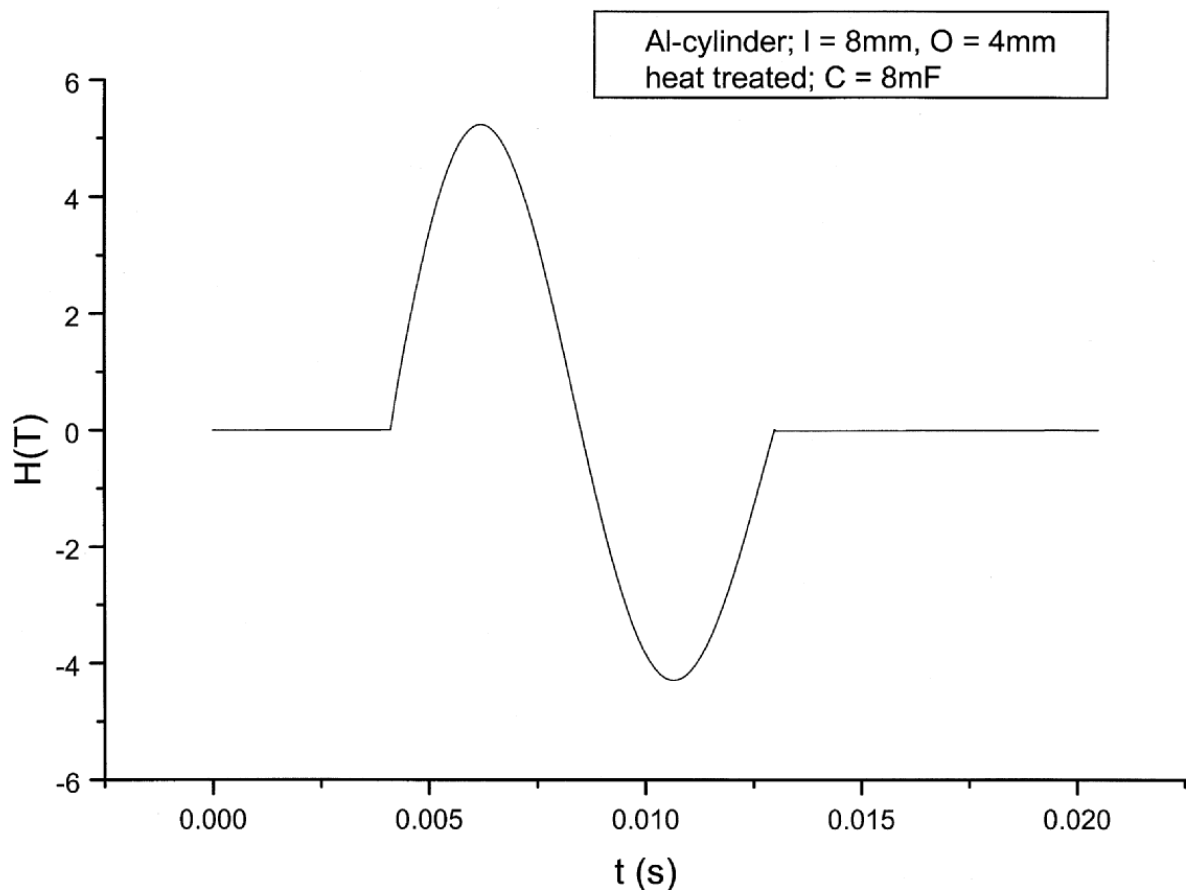


Figure 10: Magnetic field due to a current pulse in the field coil

8.1 Sample Cu1 (cylindrical)

In the experiment with the above given field, a magnetization of 94 kA/m was found at the maximum of the field.

8.1.1 Single turn coil

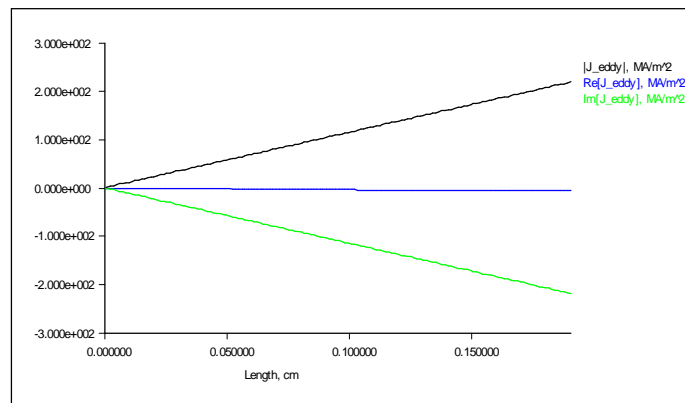
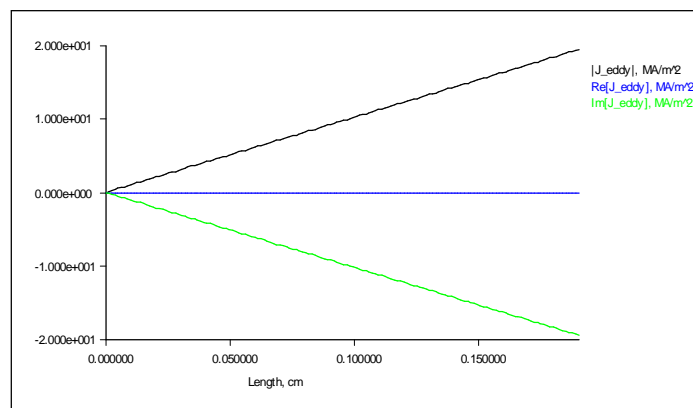


Figure 11: Complex eddy current density as a function of radial distance from axis

At a frequency of 112 Hz the maximum current density is $j_{max} = 218.8329 \text{ MA/m}^2$ and gives a magnetization of $M = 109.41645 \text{ kA/m}$. (See the following sections on how the magnetization is calculated.)

8.1.2 Coil model



**Figure 12: Complex eddy current density as a function of radial distance from axis
(10 Hz)**

At a frequency of 10 Hz the maximum current density is $j_{max} = 19.43746 \text{ MA/m}^2$ and gives a magnetization of $M = 9.71873 \text{ kA/m}$.

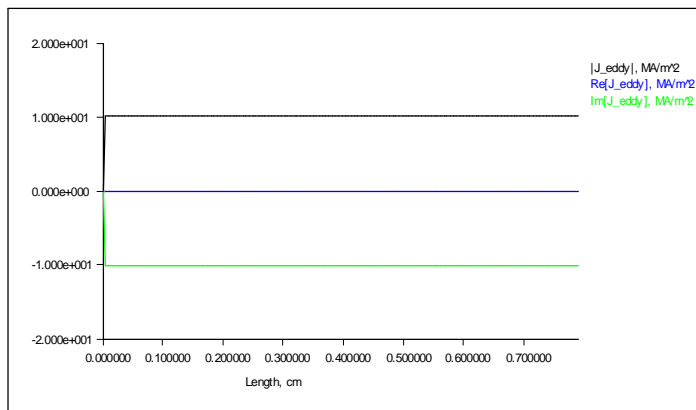


Figure 13: Complex eddy current density at a constant distance of 0.1 cm from axis (10 Hz)

It is clearly seen, that the eddy current density does not vary with the position along the symmetry axis.

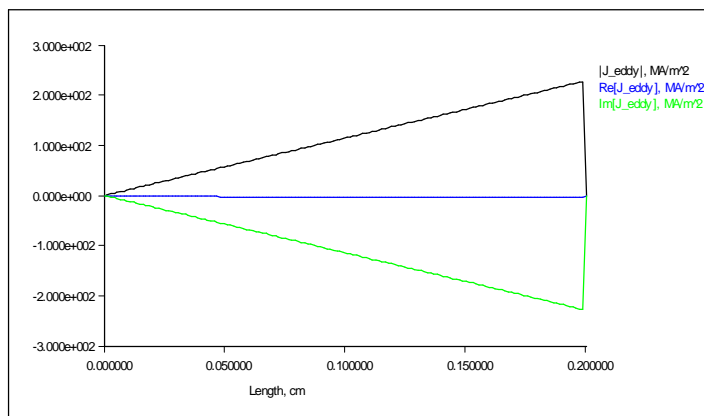


Figure 14: Complex eddy current density as a function of radial distance from axis (112 Hz)

At a frequency of 112 Hz the maximum current density is $j_{max} = 227.5316 \text{ MA/m}^2$ and gives a magnetization of $M = 113.7658 \text{ kA/m}$.

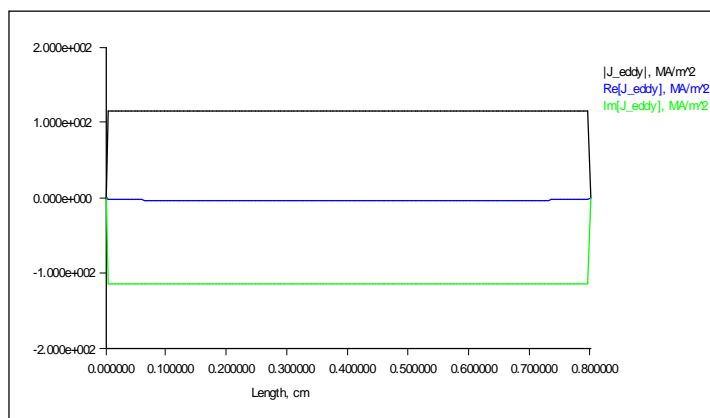


Figure 15: Complex eddy current density at a constant distance of 0.1 cm from axis

8.1.2.1 High resolution mesh

Sample Cu1, 112 Hz

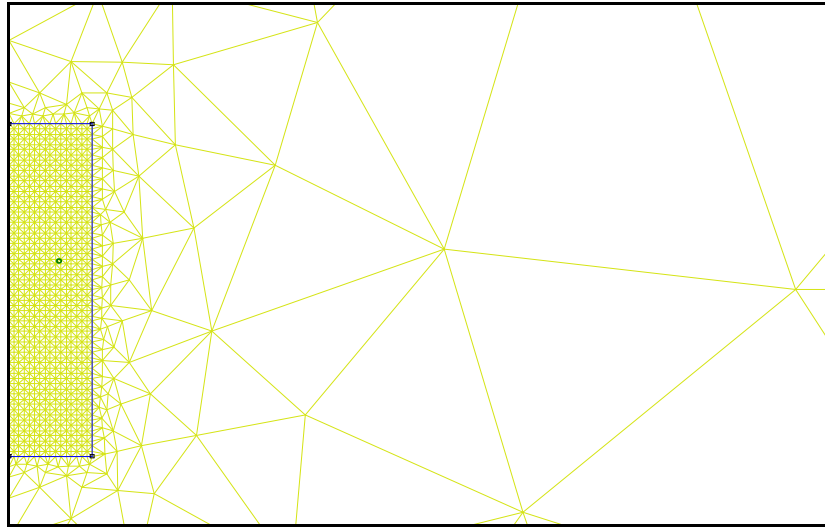


Figure 16: High resolution mesh of the cylindrical sample

The mesh consists of 6363 nodes and 12434 elements. A small portion is shown in figure 19.

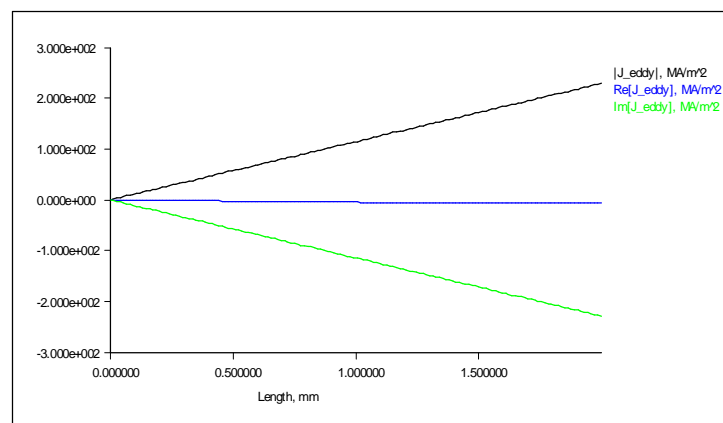


Figure 17: Complex eddy current density as a function of radial distance from axis

Figure 20 shows the perfectly linear dependence of the eddy current density on the radial distance from the symmetry axis. At the symmetry axis the eddy currents vanish, and at the circumference they reach a maximum. The amplitude of the complex eddy current is found as $(-5.180091, 228.7667)$ MA/m². Thus, the phase difference between the current in the field coil and the eddy current is $-88,70^\circ$ and the eddy currents lead the coil currents by about a quarter phase. The absolute value of the eddy currents is 228.8253 MA/m², which is in good agreement with the coarse mesh used in section 8.1.2.

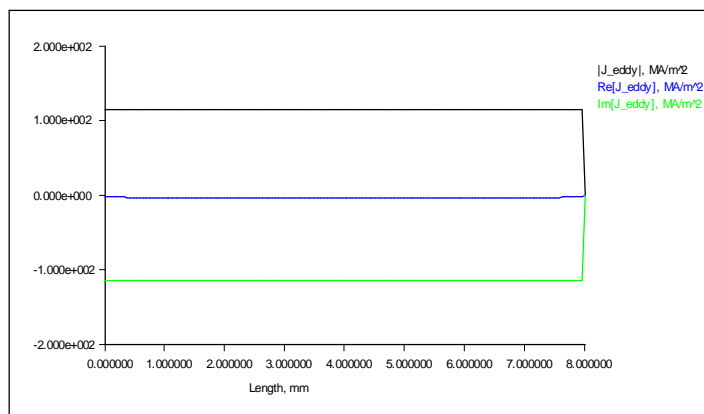


Figure 18: Complex eddy current density at constant distance from axis

Figure 15 proves, that the eddy current density is perfectly constant parallel to the symmetry axis.

8.2 Sample A13 (spherical)

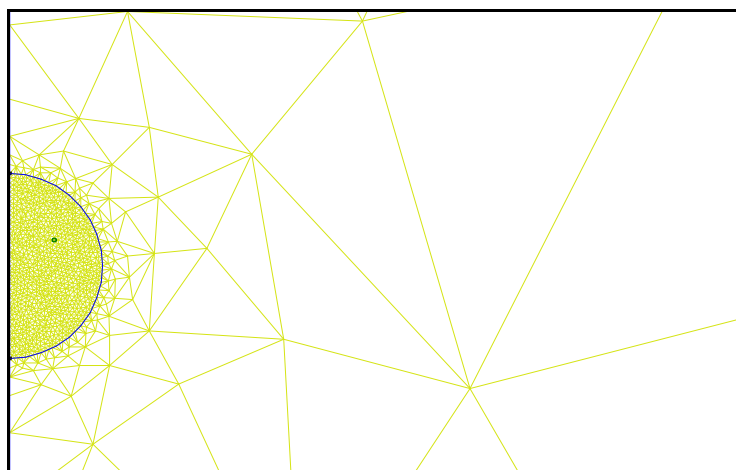


Figure 19: High resolution mesh of the spherical sample

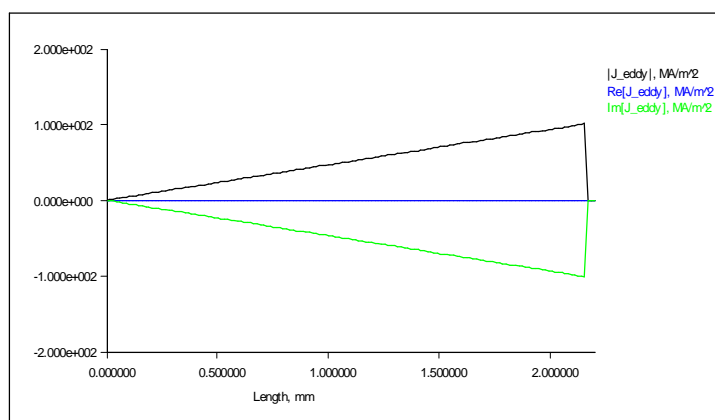


Figure 20: Complex eddy current density as a function of radial distance from axis (centre of the sphere)

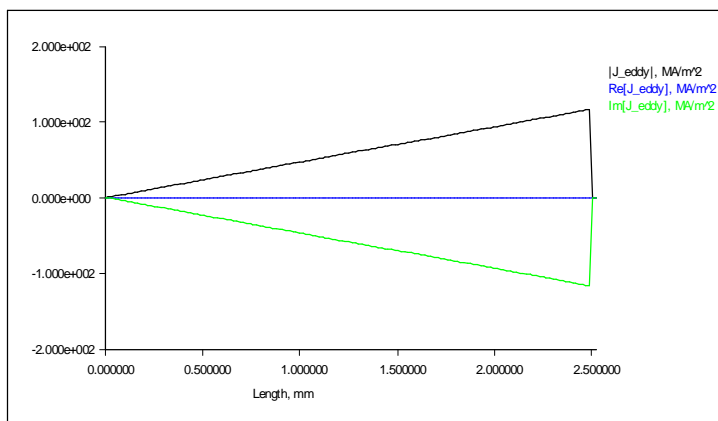


Figure 21: Complex eddy current density as a function of radial distance from axis (at $r=1.25$ mm)

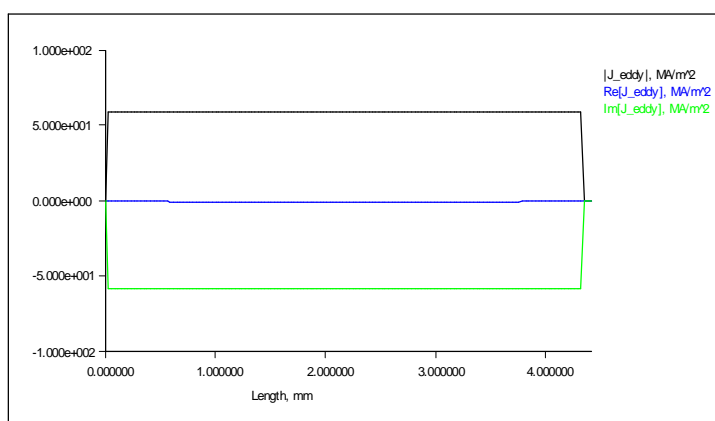


Figure 22: Complex eddy current density at constant distance from axis (1.25 mm)

8.3 Sample Cu3

7477 nodes, 14660 elements

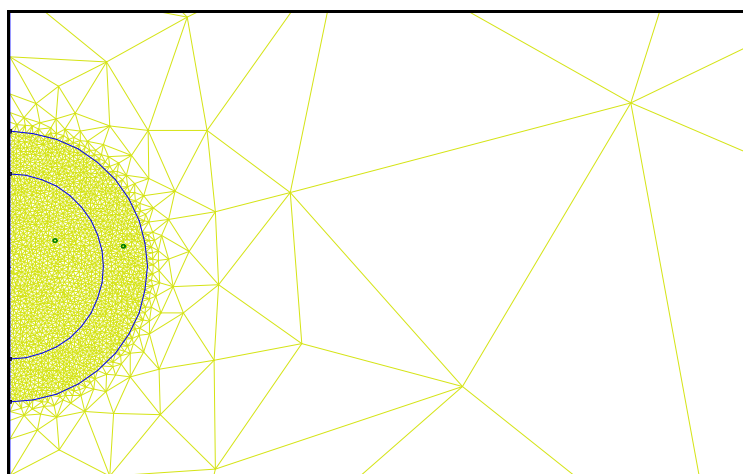


Figure 23: High resolution mesh of the spherical sample

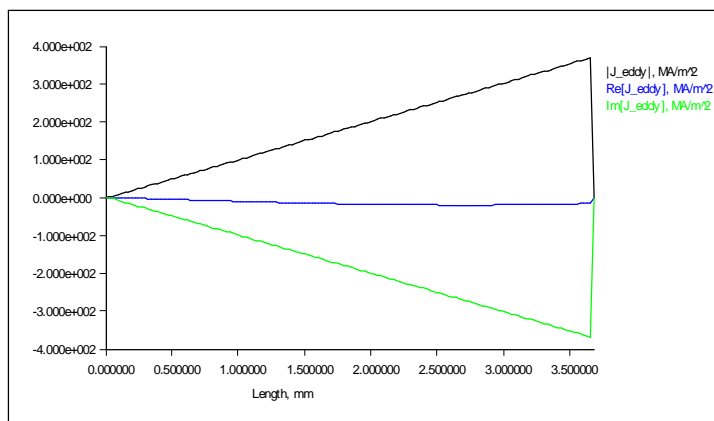


Figure 24: Complex eddy current density as a function of radial distance from axis (centre of the sphere)

8.4 Comparison of experimental and numerical results

sample units	frequency Hz	Bmax T	Mexp kA/m	Mexp/f kA/(Tm)	j_eddy_max A	Mnum kA/m	Mnum/f kA/(Tm)	Mnum/Mexp
Cu1	112	5,603		0,00	228,66	114,33	1,02	
Cu1	109,89	5,603		0,00	222,93	111,47	1,01	
Cu1	112	5,23	94	0,84	213,59	106,80	0,95	1,13613
Cu1	109,89	5,23	94	0,86	209,57	104,79	0,95	1,11474
Cu2	109,89	5,17	90	0,82	202,94	101,47	0,92	1,12744
Cu3	109,89	5,17	245,13	2,23	368,47	268,98	2,45	1,09729
Cu2	63,69	5,17	48,8	0,77	116,90	58,45	0,92	1,19774
Cu3	63,69	5,17	133,2	2,09	213,79	156,07	2,45	1,17167
Al1	112	5,23	43,335	0,39	70,79	35,40	0,32	0,81678
Al1	109,89	5,23	43,335	0,39	69,51	34,75	0,32	0,80196
Al2	109,89	5,17	37	0,34	93,53	46,77	0,43	1,26397
Al3	109,89	5,17	50	0,46	116,27	58,14	0,53	1,16271
Al2	63,69	5,17	20,9	0,33	54,21	27,11	0,43	1,29697
Al3	63,69	5,17	28,2	0,44	67,54	33,77	0,53	1,19749

Table 6: Comparison of experimental and numerical results

The agreement between experimental and numerical results is good for both cylindrical (Cu1, Cu2, Al1, Al2) and spherical (Cu3, Al3) samples.

9 Induced magnetic moment

9.1 Cylindrical samples

In order to calculate the magnetic moment, which is caused by the circular eddy currents, we have to integrate the eddy current density over the volume of the cylindrical samples (radius r_s , height h).

$$\mu = \int_0^{r_s} dr' \int_0^h dz j(r') r'^2 \pi \quad (28)$$

We have seen in figure 19, that the eddy current density is directly proportional to the radial distance from the symmetry axis. Thus, we write

$$j(r') = \frac{j_{\max} r'}{r_s}. \quad (29)$$

We obtain for the magnetic moment

$$\mu = \frac{j_{\max}}{r_s} h \int_0^{r_s} dr' r'^3 \pi = j_{\max} h \pi \frac{r_s^3}{4}. \quad (30)$$

The magnetization is given by

$$M \approx \mu/V, \quad (31)$$

where V is the volume of our cylinders

$$V = r_s^2 \pi h \quad (32)$$

Finally, we find for the magnetization

$$M = \frac{j_{\max} r_s}{4}. \quad (33)$$

Hence, the magnetization is independent of the height of the cylinder.

Since our samples have a radius r_s of 2 mm we get

$$M(\text{kA} / \text{m}) = \frac{j_{\max}}{2} (\text{MA} / \text{m}^2). \quad (34)$$

9.2 Spherical samples

In order to calculate the magnetic moment of the spherical samples, we have to integrate the eddy current density over the volume of the sphere (radius r).

$$\begin{aligned}
\mu &= \frac{1}{2} \int_V \vec{r} \times \vec{j}(\vec{r}') d\vec{r}' = \\
&= \frac{1}{2} \int_0^{r_s} \int_0^\pi \int_0^{2\pi} r' j(r', \vartheta) \sin \vartheta \cdot r'^2 \sin \vartheta dr' d\vartheta d\varphi
\end{aligned} \tag{35}$$

We have seen in figure 20, that the eddy current density is also in spherical samples directly proportional to the radial distance from the symmetry axis. Thus, we write

$$j(r', \theta) = \frac{j_{\max} r' \cos \theta}{r_s} = \frac{j_{\max} r' \sin \vartheta}{r_s} \Big|_{\vartheta=\pi/2-\theta} . \tag{36}$$

We obtain for the magnetic moment

$$\begin{aligned}
\mu &= \frac{1}{2} \int_V \vec{r} \times \vec{j}(\vec{r}') d\vec{r}' = \\
&= \frac{1}{2} \int_0^{r_s} \int_0^\pi \int_0^{2\pi} r' j(r', \vartheta) \sin \vartheta \cdot r'^2 \sin \vartheta dr' d\vartheta d\varphi = \\
&= \frac{1}{2} 2\pi \frac{j_{\max}}{r_s} \cdot \int_0^{r_s} \int_0^\pi r'^4 \sin^3 \vartheta \cdot dr' d\vartheta = \\
&= \frac{\pi j_{\max}}{r_s} \cdot \frac{r_s^5}{5} \cdot (-\cos \vartheta + 1/3 \cos^3 \vartheta) \Big|_0^\pi = \\
&= \frac{4\pi}{15} j_{\max} r_s^4
\end{aligned} \tag{37}$$

The magnetization is given by

$$M \approx \mu/V, \tag{38}$$

where V is the volume of our cylinders

$$V = \frac{4\pi r_s^3}{3} \tag{39}$$

Finally, we find for the magnetization

$$M = \frac{j_{\max} r_s}{5}. \tag{40}$$

10 Eddy currents in a solid sphere

10.1 Analytical solution

Beware:

There is a problem with this analytical solution (email from David Meeker):

From: Dcm3c@aol.com
 Date: Tue, 5 Oct 1999 01:02:53 EDT
 To: femm@egroups.com
 Subject: [femm] Re: Problems with axisymmetric problems

Thanks for the note--your writeup is pretty interesting. However, I think that femm is actually doing the correct thing in the case of the small spheres; something seems to be wrong with the analytical solution presented for this case.

To see the problem, the easiest case to consider is the one corresponding to Figure 31 (below).

In this case, a copper sphere with a radius of 3.65 mm and a conductivity of $\sigma=56.82$ MS/m is exposed to a source field of a $B_{src}=1$ Tesla amplitude varying at 109.89 Hz ($\omega=690.46$ rad/sec). This apparently corresponds to the `miniturnsphere.fem` example problem.

This is a good case to consider because the radius and frequency are small enough that the reaction field from the eddy currents can be neglected (The skin depth at this frequency and conductivity is 6.4 mm. Since the skin depth is substantially greater than the radius of the sphere, neglecting the reaction currents for the purpose of estimating the induced current density is reasonable). When you can ignore the reaction currents, you can substitute directly into Faraday's law to get an expression for the eddy current density:

$$J = -j \omega \sigma r B_{src} / 2$$

Induced Currents in a Copper Sphere at Low Frequencies

This is meant to apply when frequencies are low enough so that the radius of the sphere, R , is less than the skin depth:

$$\omega < \frac{2}{\sigma\mu R^2}$$

Faraday's Law:

$$\oint E \cdot dl = - \iint j\omega B \cdot da$$

In this case, frequencies are low enough so that we can ignore the reaction field produced by the eddy currents. Flux density B just consists of the source field, B_{src} , which is axially directed and uniform. Now, we can just substitute directly into Faraday's Law to solve for the induced currents. For some circular loop of radius r , we can write, for the right-hand side:

$$- \iint j\omega B \cdot da = -j\omega B_{src} \pi r^2$$

For the left-hand side, we can write:

$$\int E \cdot dl = \frac{2\pi r J}{\sigma}$$

Setting the two sides equal and solving for J yields:

$$J = - \left(\frac{j\omega\sigma r B_{src}}{2} \right)$$

This formula predicts an eddy current density of 71.6 MA/m² at the farthest radius of the sphere. Looking at the finite element solution, the amplitude of the induced current density at the point ($r=3.649, z=0$) is 71.63 MA/m², showing a good agreement.

Now, evaluating the sphere.nb Mathematica notebook under the above conditions yields a current 106.8 MA/m², which is substantially larger than one might expect.

So, what is the difference? I loaded sphere.nb into Mathematica and took the power series about $\omega=0$ using the Series[] function and substituted in μ_0 for μ , since we are considering the copper sphere. The result is:

$$J = -j \cdot (3/4) \cdot \omega \cdot \sigma \cdot r \cdot B_{src}$$

Now, this doesn't match the low-frequency limiting case that that one can obtain from Faraday's law. There is an extra factor of 3/2 in there for this limiting case.

For a solid sphere in a uniform sinusoidal magnetic field with an amplitude of 1 T the magnetic vector potential A can be calculated analytically [7]. In the sphere it is given by

$$A_{1\varphi}(r, \theta, \varphi) = a \cdot j_1(kr) \sin \theta \quad (41)$$

$$A_{1r}(r, \theta, \varphi) = A_{1\theta}(r, \theta, \varphi) = 0 \quad (42)$$

and in empty space it is

$$A_{2\varphi}(r, \theta, \varphi) = \left(\frac{1}{2}r + \frac{b}{r^2} \right) \sin \theta \quad (43)$$

$$A_{2r}(r, \theta, \varphi) = A_{2\theta}(r, \theta, \varphi) = 0 \quad (44)$$

where

$$a = \frac{3r_s}{2\mu_o D} \quad (45)$$

$$b = \frac{r_s^3}{D} \frac{j_1(kr_s)}{\mu_0} - \left(\frac{kr_s j_0(kr_s) - j_1(kr_s)}{2\mu} \right) \quad (46)$$

$$D = \frac{j_1(kr_s)}{\mu_0} + \left(\frac{kr_s j_0(kr_s) - j_1(kr_s)}{\mu} \right) \quad (47)$$

$j_n(\cdot)$ are the n th order Bessel functions of first kind, r_s is the radius of the solid sphere, and k is given by

$$k = (-1+i) \sqrt{\frac{\omega\mu\sigma}{2}} \quad (48)$$

10.2 Numerical solution

A solid iron sphere with radius $r_s = 5$ cm, $\mu_r = 20$, $\sigma = 10$ MS/m in a sinusoidally varying magnetic field with an amplitude of 1 T and a frequency of 50 Hz was simulated. The external field was generated by the well known field coil and its current suitably rescaled. Therefore, the magnetic field is not perfectly homogeneous. The finite element mesh consisted of 9324 nodes and 18319 elements.

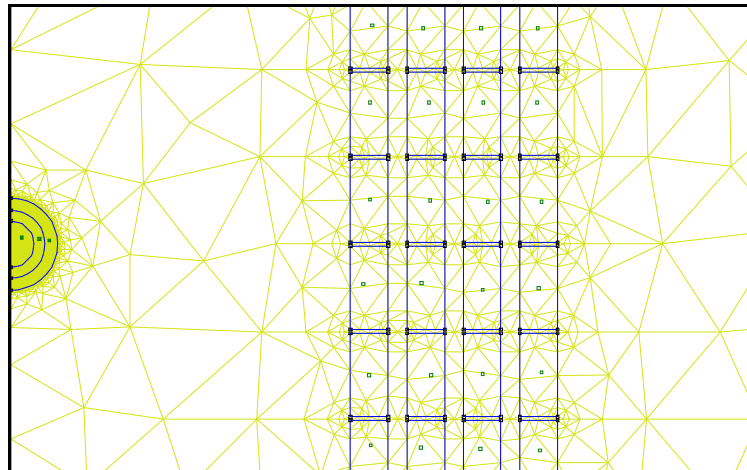


Figure 25: FE mesh (small cut out) of the iron sphere and detailed coil model

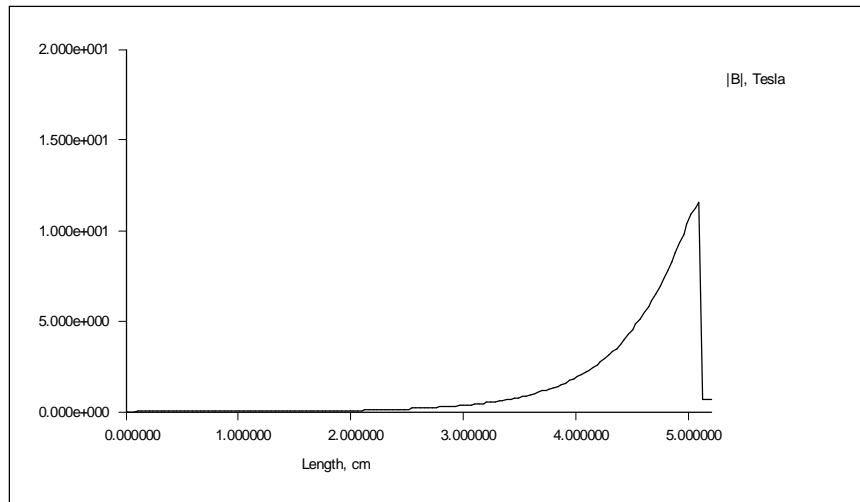


Figure 26: Magnetic induction in the iron sphere

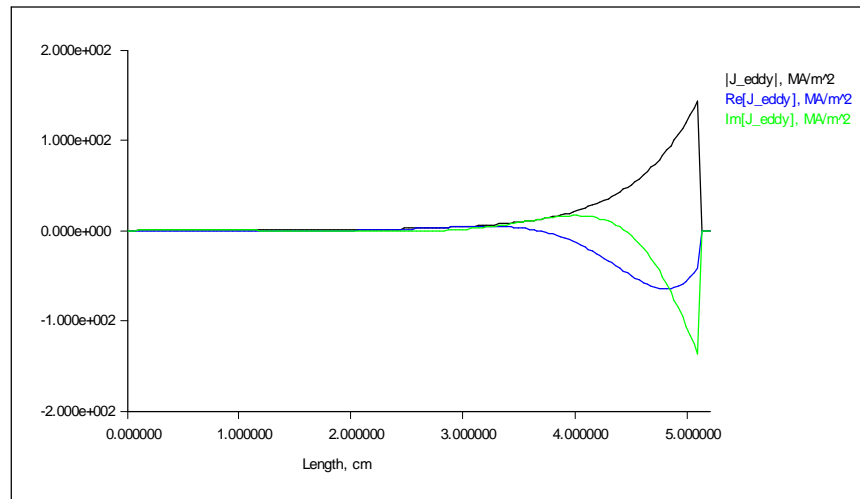


Figure 27: Eddy current density in the iron sphere

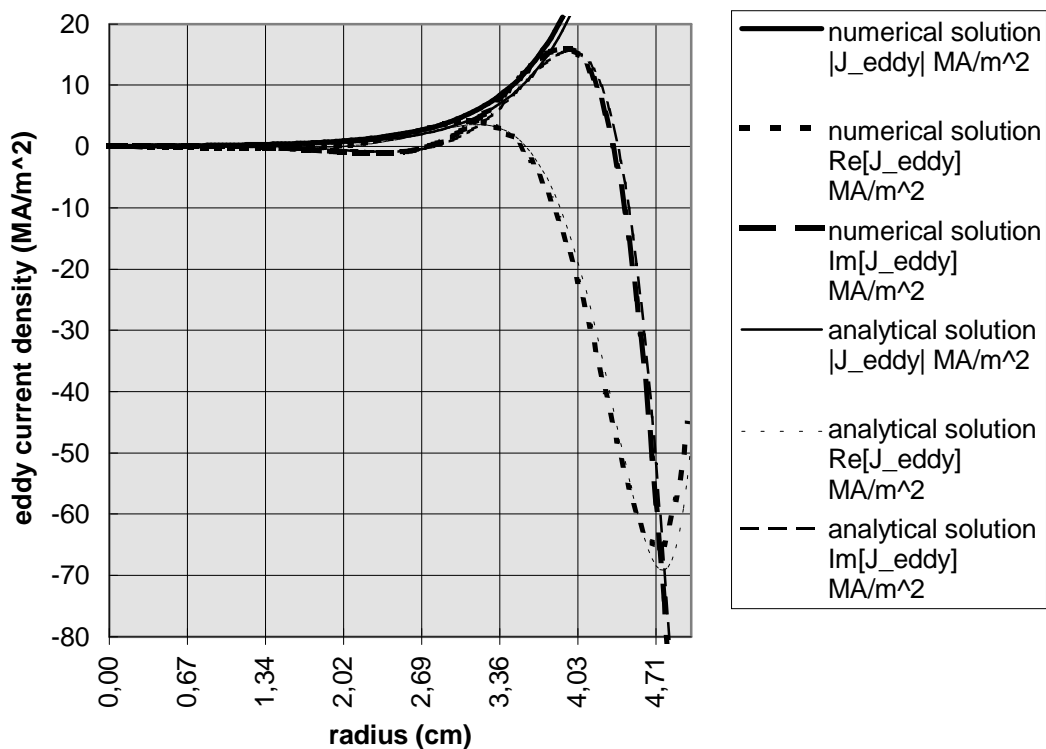


Figure 28: Eddy current density in the iron sphere

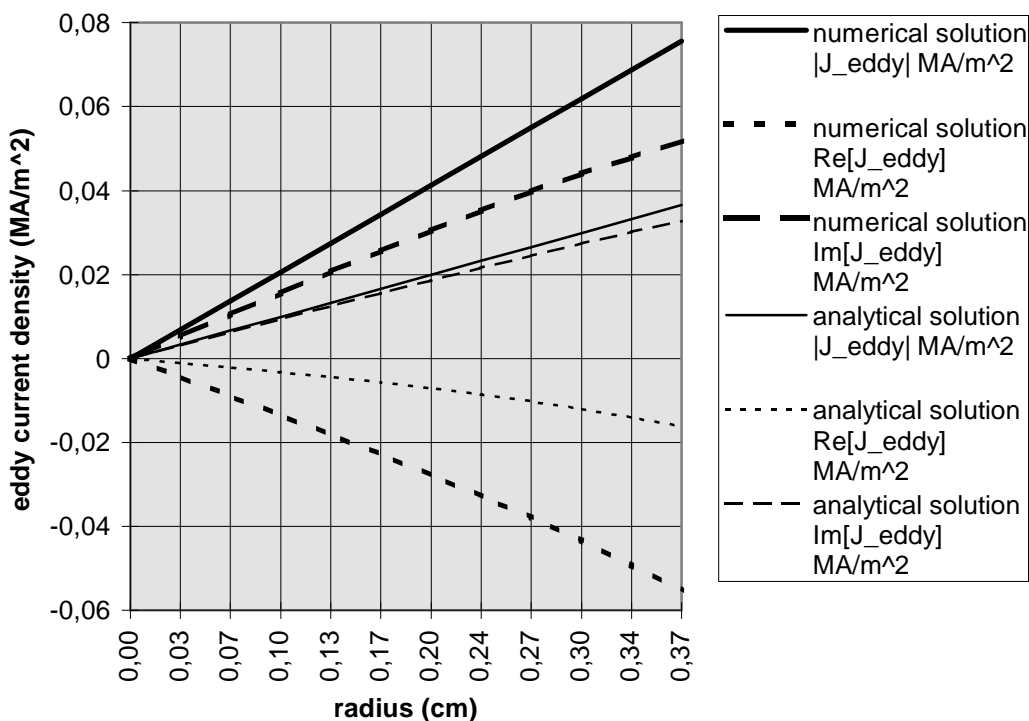


Figure 29: Eddy current density in the iron sphere

10.3 Sample Cu3

The results for the spherical Copper sample Cu3 in a sinusoidally varying field of 1 T shows a rather large deviation from the analytic results. It has been verified, that the asymptotic boundary conditions do not account for that. Even if the radius of the spherical boundary, where asymptotic boundary conditions apply, is doubled, the results remain almost identical (they cannot be distinguished in the plots below). Also the simple model of the field coil (the single turn coil) leaves the result unchanged. Even if the diameter of the field coil and its height are doubled to improve the homogeneity of the field, no difference in the result can be found.

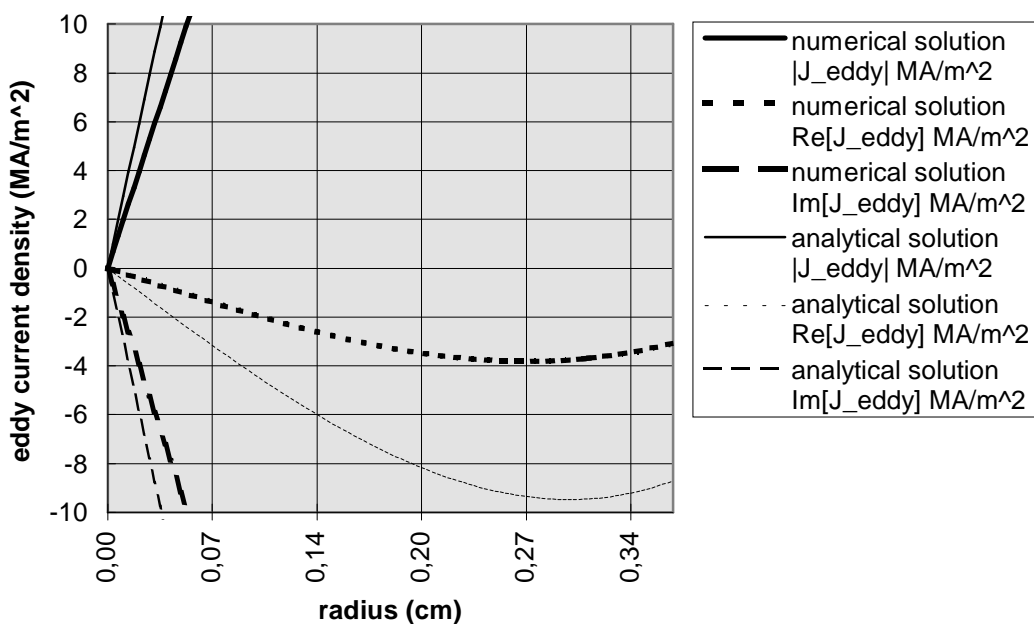


Figure 30: Eddy current density in sample Cu2 @ 1 T

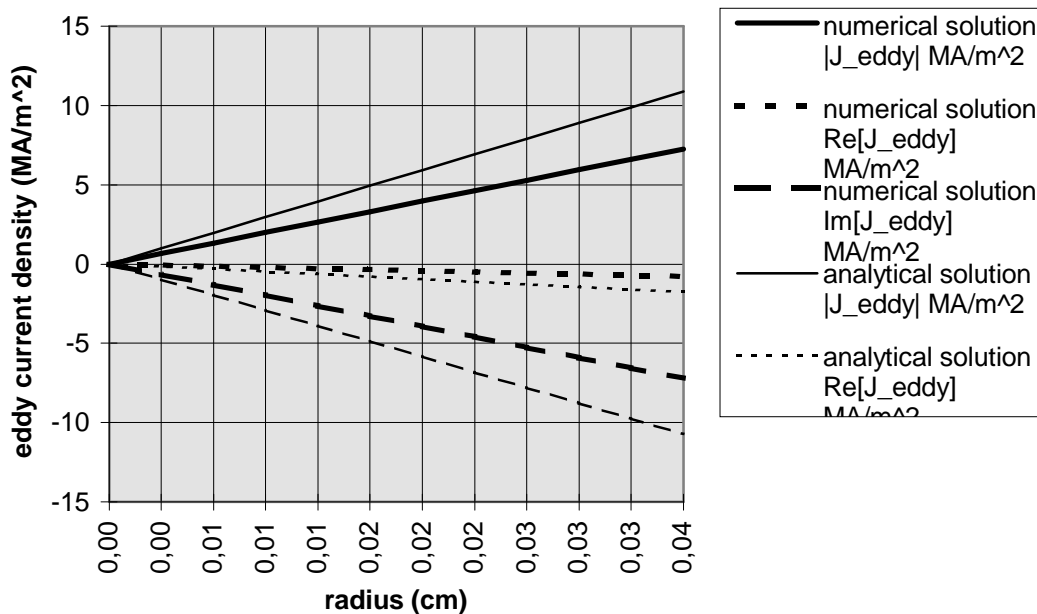


Figure 31: Eddy current density in sample Cu2 @ 1 T

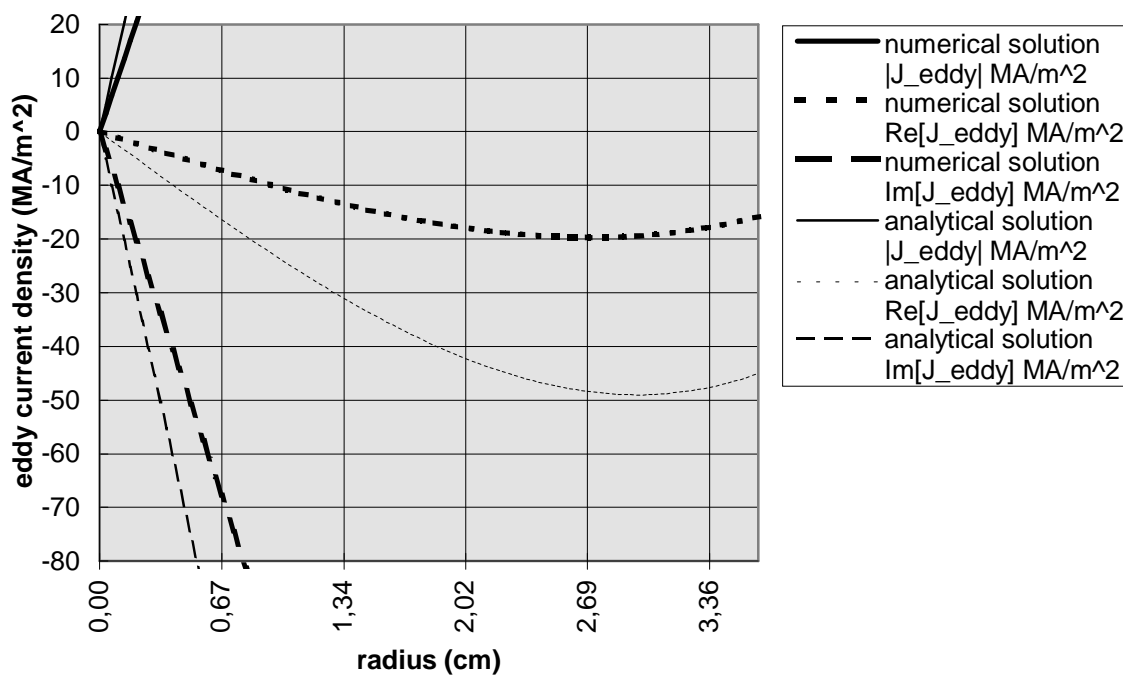


Figure 32: Eddy current density in sample Cu2 @ 5.17 T

10.4 Frequency dependence

The frequency dependence of the magnetization is shown in the following table (data analyzed and collected by Prof. Grössinger). The magnetization has been plotted as a function of $\frac{\partial B}{\partial t}$

and the results analyzed by linear regression. The offset gives the value of M for $\frac{\partial B}{\partial t} = 0$,

where the magnetization should vanish. However, these values are acceptable, if we take into account, that the magnetization is typically of the order of 100 kA/m.

sample	shape	height	diameter	weight	capacity	U	offset	error	slope	error
Cu	sphere		7,3 mm	1,81008 g	8 mF	2000 V	1518,787	315,574	-9,670E-06	1,791E-06
Cu	sphere		7,3 mm	1,81008 g	24 mF	1180 V	-2966,477	55,342	-9,236E-06	5,583E-06
Cu	cylinder	8 mm	4 mm	0,90926 g	8 mF	2000 V	693,263	32,656	-3,505E-06	1,820E-06
Cu	cylinder	8 mm	4 mm	0,90926 g	24 mF	1180 V	-322,684	13,094	-3,435E-06	1,306E-06
Al	sphere		5 mm	187,7 mg	8 mF	2000 V	716,247	18,547	-1,978E-06	1,026E-06
Al	sphere		5 mm	187,7 mg	24 mF	1180 V	-1919,135	26,116	-1,885E-06	2,596E-06
Al	cylinder	8 mm	4 mm	280,55 mg	8 mF	2000 V	1167,680	10,552	-1,500E-06	5,840E-06
Al	cylinder	8 mm	4 mm	280,55 mg	24 mF	1180 V	-1272,926	10,050	-1,403E-06	9,986E-06

Table 7: Comparison of experimental and numerical results

11 Comments on release 2.1a of FEMM

Copied from <http://members.aol.com/gmagnetics/changes.htm>:

Changes from 2.1 to 2.1a - September 11, 1999

- This is mostly a bug fix version. No obvious functionality has been added to the program. However, quite a lot of work has gone on "under the hood" to fix some bugs that cropped up and to give more accurate answers.
- Several integrals had errors when applied to axisymmetric problems. These errors have now been fixed. The specific integrals modified are:
 - Total losses--forgot to multiply by $2\pi r$
 - Total current--modified to include induced currents in the integration. Previously, only source currents were included.
- The formulation used to solve axisymmetric problems has been changed. The old formulation gave good performance almost all of the time, but occasionally, a problem would come along in which the scheme would exhibit poor convergence. The formulation has been changed to one similar to the axisymmetric formulation suggested by Henrotte et al. in their paper "A new method for axisymmetric linear and nonlinear problems," IEEE Trans. Mag. 29(3):1332-1335, March 1993. This formulation has the same well-behaved characteristics as the old formulation in the region close to the $r=0$ line, but it also successfully deals with the problems in which the old formulation gave spurious results. The new formulation has been applied to both static and harmonic problems in femm. The wrong eddy currents were reported in response to inquiries about solution properties at a particular point in the axisymmetric case. Some typographical errors in the manual were fixed.

This new release has been tested on a few problems, and it was found, that the postprocessing tool `femmview` does not display the results properly any more. The eddy current density seems not to be proportional to the radius (for small distances of a few millimetres) any more, but to be almost constant with a non-vanishing value for $r=0$. However, the the old version (2.1) of `femmview` can be used with the new release of `femme` and `fkern`. The preprocessing and FE programs `femme` and `fkern` seem to work properly. For the solid iron sphere and the small copper sphere identical results have been obtained with the old and new versions.

The remark in the above given notes for the new release on the behaviour of the solution in the region close to $r=0$ seems to be noteworthy. Probably this is a known problem in the solution of axisymmetric electromagnetic problems, because the solution "far away" from the axis (as is the case for the 5 cm iron sphere) is in good agreement with the analytical solution. Close to the symmetry axis both, the FE solution of the iron sphere and that of the copper spheres shows rather large deviations for the analytical solution.

12 Conclusions

Eddy currents, which are induced in a conductor by a non-steady external magnetic field, have been calculated and compared with experimental results. The analytical solution for spherical samples has been found to agree very well with the numerical results of the finite element package FEMM for large samples (the iron sphere). For small samples and at small distances from the symmetry axis rather large deviations have been found. The analytical solution is about twice as high as the numerical solution for the copper sphere. However, the numerical solution is still about twice as high as the experimentally found magnetic moment.

The agreement between numerical and experimental results is better for cylindrical samples.

There are a few remarkable aspects about the analytical solution for spherical samples:

- Only a , b , and D are functions of r_s , the radius of the sphere. Since $A_{1\varphi}$ is proportional to a the radius r_s influences only the scaling of $A_{1\varphi}$ and therefore of the eddy currents.
- The “shape” of the real and imaginary parts of $A_{1\varphi}$ is always given by the Bessel function $j_1(kr)$. Only k , which is a function of the frequency, the magnetic permeability, and the conductivity, enters into the Bessel function.

13 References

- [1] Charles W. Steele, *Numerical computation of electric and magnetic fields*. Van Nostrand Reinhold, New York, 1987
- [2] J. Jin, *The finite element method in electromagnetics*. New York: Wiley, 1993
- [3] D. Meeker, Finite Element Method Magnetics, URL:
<http://members.aol.com/dcm3c>
- [4] B.M. Jaworski, A.A. Detlaf, *Physik griffbereit*. Braunschweig: Vieweg, 1972
- [5] B. Streibl, "Dynamische mikromagnetische Simulation von mumag Standardproblemen", Diplomarbeit, TU Wien, 1998
- [6] WebElements, URL: <http://www.webelements.com>
- [7] T. Morisue, M. Fukumi, "3-D eddy current calculation using the magnetic vector potential." *IEEE Trans. Magn.*, vol. 24, no. 1, pp.106-109, 1988

Additional references

- [A] International Compumag Society, URL: <http://ics.ec-lyon.fr/>
- [B] Testing Electromagnetic Analysis Methods (T.E.A.M.),
URL: <http://ics.ec-lyon.fr/team.html>
- [C] R. Albanese, G. Rubinacci, "Solution of three dimensional eddy current problems by integral and differential methods." *IEEE Trans. Magn.*, Vol. 24, No. 1, January 1988, pp. 98-101.
- [D] O. Biro, "Use of a two-component vector potential for 3-D eddy current calculations." *IEEE Trans. Magn.*, Vol. 24, No. 1, January 1988, pp. 102-105.
- [E] W. Renhart, H. Stögner, K. Preis, "Calculation of 3D eddy current problems by finite element method using either an electric or a magnetic vector potential." *IEEE Trans. Magn.*, Vol. 24, No. 1, January 1988, pp. 122-125.
- [F] T. Misaki and H. Tsuboi, "Techniques for boundary element analysis of three-dimensional eddy current distribution." *IEEE Trans. Magn.*, Vol. 24, No. 1, January 1988, pp. 146-149.
- [G] , " ." *IEEE Trans. Magn.*, Vol. 24, No. 1, January 1988, pp. 431-434.
- [H] T.P.Theodoulidis, C.S.Antonopoulos, E.E.Kriezis, "Analytical Solution for the eddy current problem inside a conducting cylinder using the secont order magnetic vector

potential.” *International Journal for Comput. and Math. in Electrical and Electronic Engineering*, Vol. 14, No. 4, 1995, pp. 45-48.

- [I] T. Nakata, N. Takahashi; K. Fujiwara, “Summary of results for benchmark problem 10 (steel plates around a coil).” *The International Journal for Computation and Mathematics in Electrical and Electronic Engineering*. vol.14, no.2-3; Sept. 1995; p.103-12.

Abstract: Benchmark problem 10 of the TEAM workshop consists of steel plates around a coil (nonlinear transient eddy current problem). Eight computer codes are applied, and nine solutions are compared with each other and with the experimental results.

- [J] T. Nakata, N. Takahashi; K. Fujiwara, “Summary of results for TEAM Workshop problem 13 (3-D nonlinear magnetostatic model). ” *The International Journal for Computation and Mathematics in Electrical and Electronic Engineering*. vol.14, no.2-3; Sept. 1995; p.91-101.

Abstract: Seven computer codes developed by five groups are applied to the benchmark problem 13 of the TEAM workshop which consists of steel plates around a coil (a nonlinear magnetostatic problem). The solutions are compared with each other and with experimental results.

- [K] H. T. Yu, K. R. Shao, K. D. Zhou, J. D. Lavers, “H method for solving 3D eddy current problems.” *IEEE Trans. Magn.*, vol.31, no.6, pt.2; Nov. 1995; p.3518-20.

Abstract: A novel finite element model, which uses magnetic field intensity H as a state variable in the whole solution region of 3D eddy current problems, is presented. A surface integral on the interface, which leads to asymmetric equations in discretization, is considered in this formulation. The formulation uses consistently linear edge elements and flux continuity is ensured by imposing $\text{Del} \cdot B=0$ with the penalty method. Numerical results of the problem No. 3 of the Team Workshop are provided, showing the validity of the algorithm.

- [L] D. Lavers, I. P. Boglaev, V. V. Sirotkin, “Domain decomposition technique for 2-D eddy current problem.” IEEE CEFC ' 96. The Seventh Biennial IEEE Conference on Electromagnetic Field Computation. IEEE, New York, NY, USA; 1996; 498 pp. p.475.

Abstract: Numerical solution of 2-D eddy current problem for an infinitely long conductive cylinder in a transverse oscillating field is considered. A domain

decomposition algorithm suitable for parallelization is described. Numerical experiments are presented.

- [M] Filtz, A. Nethe, "Some remarks on solving the problem of three-dimensional eddy currents in circular cylinders of finite length." *Archiv für Elektrotechnik*, vol.76, no.3; 1993; p.195-200.

Abstract: The authors describe an analytical method to calculate three-dimensional eddy currents in a circular cylinder with finite dimensions. An examination of papers on this topic shows that some of them contain grave mistakes which are discussed in detail. The authors show that the disappearance of the normal component of the current density on the cylinder end faces is a necessary boundary condition but is, however, by no means sufficient. Moreover, in contrast to an infinitely long cylinder an additional TEM-field has to be taken into account. Finally, the solution method is practically applied to the example of a turbogenerator model and the results are compared with the values found in other references.

14 List of models

14.1 Subdirectory test

14.1.1 `turn.FEM`

This model consists of a very thin single turn coil (2×2 mm) with an inner radius of 50 mm. It has been used to compare the solution of `femme` with the analytic result for a circular current.

14.1.2 `coilturn.FEM`

This model consists of the above described thin single turn coil and a model of the field coil, which is used in the experimental setup.

14.2 Subdirectory experiment

14.2.1 `singturn.FEM`

This model includes the simplified model of the field coil (only one big turn) and a cylinder with a radius of 2 mm and a height of 8 mm.

14.2.2 `singturnsphere.FEM`

This model includes the simplified model of the field coil (only one big turn) and spheres with radii of 2.5, 3.65, and 5 length units.

14.2.3 `singturnfsphere.FEM`

This model includes the simplified model of a field coil (only one big thin turn) at a larger distance and spheres with radii of 2.5, 3.65, and 5 length units.

14.2.4 `cylinder.FEM`

This model includes the above described cylinder and the detailed model of the field coil (4×24 turns) used in the experimental setup.

14.2.5 `sphere.FEM`

This model includes the detailed coil model and three spheres (radius of 2.5, 3.6 mm, and 5 cm) for the spherical Cu and Al samples. Furthermore, it has been used to compare the solution of `femme` with the analytic result for the eddy currents in a solid Fe sphere [7].

14.2.6 `miniturnsphere.FEM`

This model includes the simplified model of a field coil (only one small thin turn) at a short distance.

14.2.7 `spheref.FEM`

This model is the same as `sphere.FEM`, but the radius of the boundary, where asymptotic boundary conditions are applied, is doubled.

15 Appendix

15.1 *Mathematica package sphere.nb*

15.2 *David Meeker, Finite Element Method Magnetics. User's Manual*

This is the manual for David Meeker's FE package [3].